CHAPTER 3

ELECTRONIC STRUCTURES OF PRISTINE PEROVSKITES

Solutions obtained from Khon-Sham equation provide the electronic structures of a given many body system. These electronic structures then lead to extraction of several characteristics, such as optical, chemical, and electrical properties, for constructing fundamental understanding of the systems of interest. Therefore, it is important for this thesis to firstly perform the electronic structure calculation of pristine perovskites before moving to the investigation of piezoelectric properties and morphotropic phase boundary of their solid solutions.

In this chapter, the electronic structures, i.e. band structures and density of states (DOS) of $KNbO_3$, $NaNbO_3$, $AgNbO_3$, $BiGaO_3$, and $BiAlO_3$ are provided. For band structure calculation, the Kohn-Sham eigenvalues need to be aligned along high symmetry path of irreducible Brillouin zone. Choice of any two high symmetry points and the direction of path connecting them are arbitrary. Thus, the feature of band structure of any materials is not unique due to many possible ways to assign high symmetry path. However, for the path connecting the same couple of high symmetry points (e.g. Γ to X), the obtained band structure should be identical in the same materials.

For the DOS calculation, DOS in energy domain is generally defined as the number of electronic states between infinitesimal interval of the considered energy range. The electronic states (which are directly proportional to number of electrons) are obtained from all k-points defined in calculation. Note that the k-points should be sampling according to the definition of the electronic wave function in Bloch form, and should be distributed homogeneously. Therefore, the feature of DOS (in presenting the distribution of electronic states as a function of energy) is unique and does not depend only on the choice of high symmetry path of Brillouin zone, because it is summed from all considered k-points. Details of band structures and density of states of $KNbO_3$, $NaNbO_3$, $AgNbO_3$, $BiGaO_3$, and $BiAlO_3$ can be found in the subsequent sections.

3.1 Electronic structures of $KNbO_3$

At room temperature, $KNbO_3$ adopts orthorhombic crystal structure with *Bmm2* space group. Its primitive unit cell contains 10 atoms (two formula units of $KNbO_3$). The crystal structure of $KNbO_3$ is usually defined with lattice parameters, $c > a > b$, and can be represented as shown in Figure 3.1.

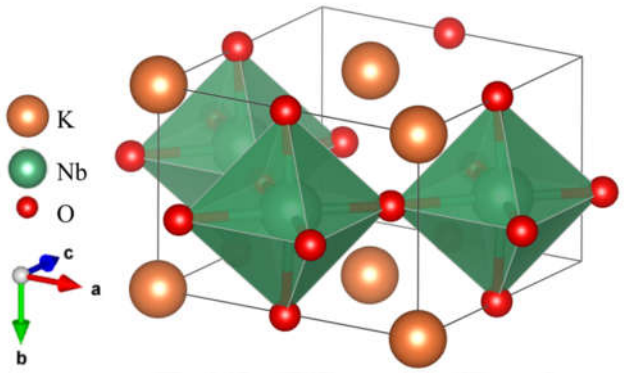

Figure 3.1 Crystal structure of $KNbO_3$ in *Bmm2* space group. Nb atoms are confined in oxygen octahedral cages, so their displacement can be measured with respect to the surrounding O atoms.

The crystal structure of $KNbO_3$ shown in Figure 3.1 is a result of equilibrium DFT calculation. The calculation was performed using plane wave pseudopotential method implemented in PWscf package [45]. Pseudopotentials used to describe electron-ion interaction of K, Nb, and O atoms were obtained from GBRV library (Garrity, Bennett, Rabe, and Vanderbilt) [46]. 4×6×4 k-point mesh was considered to provide sufficient density of k-point for Brillouin zone integration. The kinetic energy cutoff of 60 Ry was used to truncate the number of plane wave basis (55,000 basis in this case) and was found to yield the reasonable results. This choice of the k-point mesh and the kinetic energy cutoff of orthorhombic $KNbO_3$ was determined from the energy convergence test as shown in Figure 3.2.

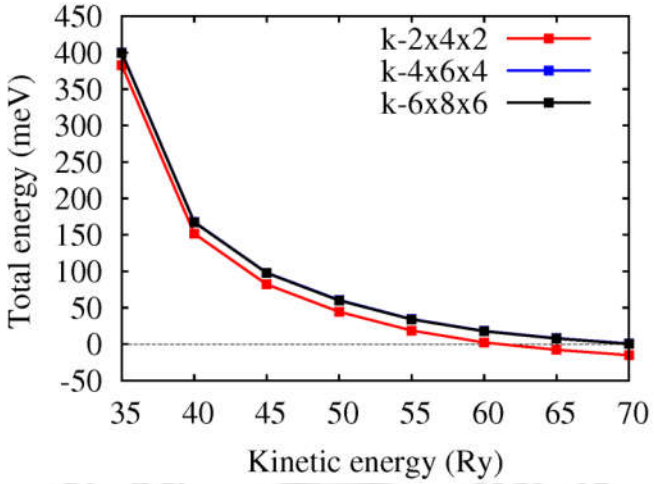

Figure 3.2 Convergence tests of DFT parameters with respect to total energy. Total energy was acquired from the calculation using 6×8×6 of k-point mesh, where 70 Ry of energy cutoff was set to zero energy level for conveniences in the comparison.

From Figure 3.2, it can be noticed that using 4×6×4 and 6×8×6 k-point mesh yield exactly the same $KNbO_3$ total energy (they lie on each other) along the considered kinetic energy cutoff range (35-70 Ry). Hence, 4×6×4 k-point mesh provides sufficient density of k-point for Brillouin zone integration. Similarly, the calculation performed at 60 Ry of energy cutoff yields the total energy comparable with that from using 70 Ry. The energy difference of about 10-20 meV in energy cutoff test is usually found to give no difference in the calculated results. This is because, for the use of plane wave expansion with high energy cutoff, the difference in total energy (from different cutoff) can be typically considered as a shift in energy reference. Further, the kinetic energy cutoff for pseudopotentials in GBRV library was suggested not to be smaller than 40 Ry. Therefore, the use of 60 Ry energy cutoff is appropriate.

After the reliable DFT parameters have been obtained, the calculation of electronic structures of $KNbO_3$ can be performed. For band structure calculation, the electronic states near band gap has to be carefully investigated because electron near the valence band maximum (VBM) have stronger chemical interaction and give higher contribution to chemical and physical properties of materials than the electrons in the deeper orbital. Energy band structure of $KNbO_3$ in *Bmm2* space group can be represented as shown in Figure 3.3.

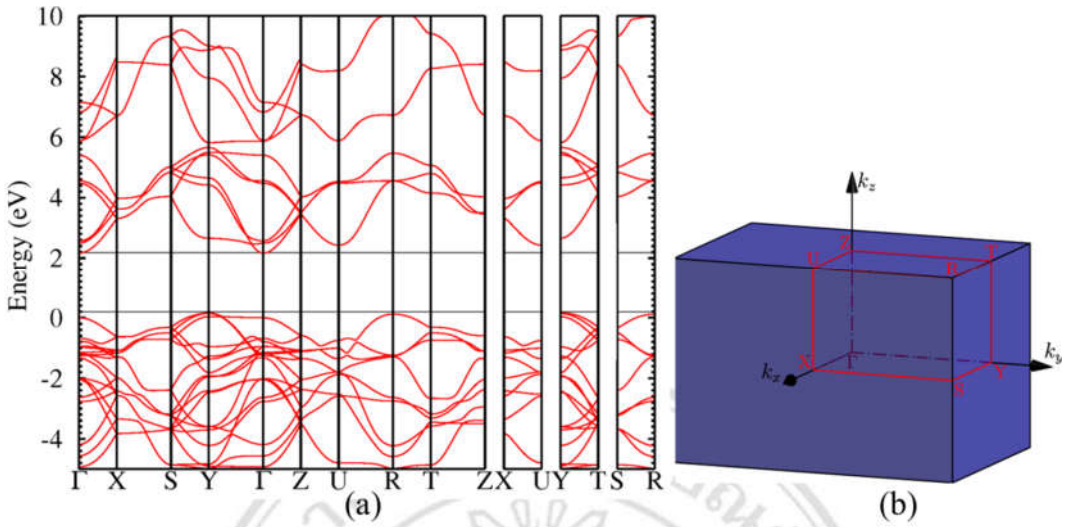

Figure 3.3 (a) The electronic band structure of orthorhombic $KNbO_3$ along full symmetry path of irreducible Brillouin zone, and (b) the irreducible Brillouin zone (bounded by red lines) and the associated high symmetry points (labeled in red) used for band structure calculation. Zero of energy was set as a part of VBM at Γ point.

As is seen in Figure 3.3, orthorhombic $KNbO_3$ has been predicted to be semiconductor under the generalized gradient approximation (GGA) in the exchange interaction [47]. Band gap calculated based on GGA is well-known to be smaller than that of the experimental value. However, other band structure-related properties, including direct/indirect character of band gap are still comparable within the use of GGA framework, e.g. see Table II in Ref. [48] and Tables I and III in Ref. [49]. Our calculated results then indicate that $KNbO_3$ possesses indirect band gap from Y to Γ point. This obtained result is consistent with the results from Ref. [50], where their GGA band gap of $KNbO_3$ is indirect as shown in Figure 11(E) in their article [50]. In addition, their predicted band gap of 2.10 eV is comparable with our result which is 1.98 eV.

To further investigate the electronic contribution to the states near band gap, the density of states (DOS) and projected density of states (PDOS) of $KNbO_3$ are analyzed as shown in Figure 3.4 .

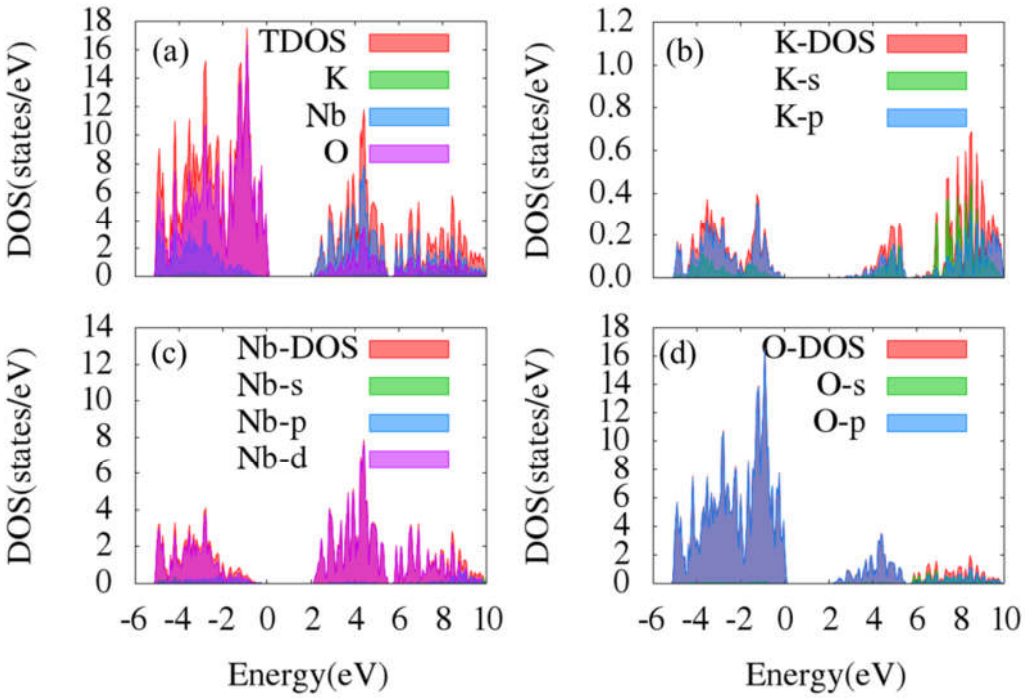

Figure 3.4 Density of states (DOS) of orthorhombic $KNbO_3$: (a) total DOS and summation of DOS of K, Nb, and O atoms, (b) DOS of K atom and its projection onto *s* and *p* orbitals, (c) DOS of Nb atom and its projection onto *s*, *p*, and *d* orbitals, and (d) DOS of O atom and its projection onto *s* and *p* orbitals.

Form Figure 3.4, it can be noticed that the main contribution of electronic states near band gap of $KNbO_3$ are from Nb and O atoms. The contribution from K atom is low as it can be seen in Figure 3.4 (b). To consider DOS of Nb and O atoms individually, most of electronic states near band gap of Nb are from 4*d* orbital while those of O are from 2*p* orbital. Therefore, this high contribution of Nb 4*d* and O 2*p* indicates their important roles on chemical and physical properties of $KNbO_3$. However, the main peak of Nb 4*d* is in conduction band region while O 2*p* display its peak in the region of valence band. It is known that the overlapping between electronic states from different atomic orbitals can be interpreted as their hybridization. However, Nb 4*d* and O 2*p* exhibit the peaks in the different energy range, so the hybridization between them is then not very strong. This probably leads to a fairly small displacement of Nb from center of oxygen octahedral cage as shown in Figure 3.1. Since large displacement of cation with respect to anion usually introduces strong polarization, the polarization of $KNbO_3$ is then quite low compared with that of $PbTiO_3$ [51] or $BiFeO_3$ [52]. Modifying

$KNbO_3$ by the incorporation of atom with significantly shorter ionic radius, such as Li, may cause stronger distortion probably leading to the improvement of polarization as suggested in Ref. [53].

3.2 Electronic structures of $NaNbO_3$

$NaNbO_3$ perovskite is often observed in orthorhombic crystal structure with *Pbcm* symmetry. With this type of symmetry, its primitive unit cell contains 40 atoms (8 formula units of $NaNbO_3$) as shown in Figure 3.5.

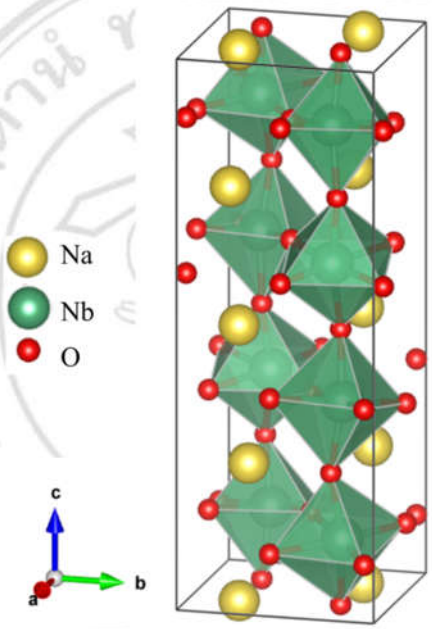

Figure 3.5 Primitive unit cell of $NaNbO_3$ perovskite in *Pbcm* space group, where the oxygen octahedral cages confine Nb atoms on the B-site of the perovskite structure.

The crystal structure of $NaNbO_3$ represented in Figure 3.5 has been relaxed to its equilibrium structure using DFT calculation within GGA approach and pseudopotentials from Ref. [46]. To considered if DFT results are reliable for $NaNbO_3$, the density of k-point and kinetic energy cutoff were tested for their convergence with respect to the total energy. Based on the same procedure used in the former case, the convergence tests of DFT parameters for the electronic structure calculation of $NaNbO_3$ can be presented in Figure 3.6.

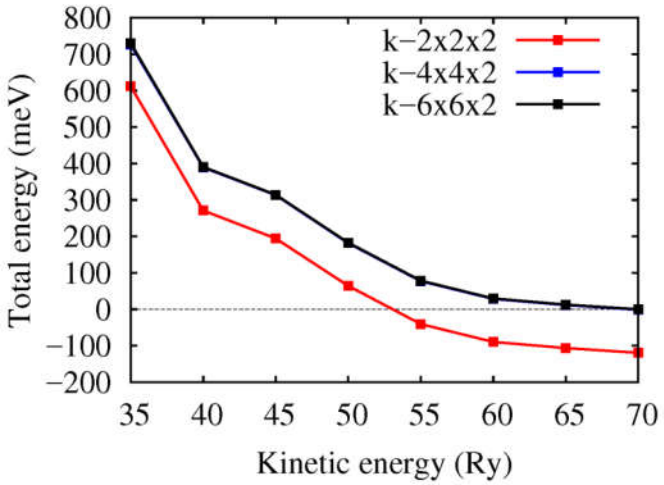

Figure 3.6 The convergence tests of k-point mesh and kinetic energy cutoff with respect to total energy of $NaNbO_3$. The total energy was obtained from the calculation using 6×6×2 k-point mesh, where 70 Ry of kinetic energy cutoff was set to zero energy level for conveniences in the comparison.

Figure 3.6 reveals that the use of 4×4×2 k-point mesh reproduces the same values of total energy as in the case of using 6×6×2 k-point mesh (as lying on top of each other). As number of k-point used for each direction in reciprocal space is inversely proportional to length of direct lattice, larger unit cell then requires lower number of k-point. Therefore, the z-component of k-point mesh applied in this case can be set very small because the lattice parameter *c* of $NaNbO_3$ is largely extended. For kinetic energy cutoff, which directly relates to the choice of pseudopotentials used, the convergence tests suggested that 60 Ry for the cutoff is acceptable. Next, with these obtained reliable calculation parameters, the electronic structure calculation of $NaNbO_3$ perovskite can then be performed using this set of parameters. The results for electronic band structure can be represented as shown in Figure 3.7.

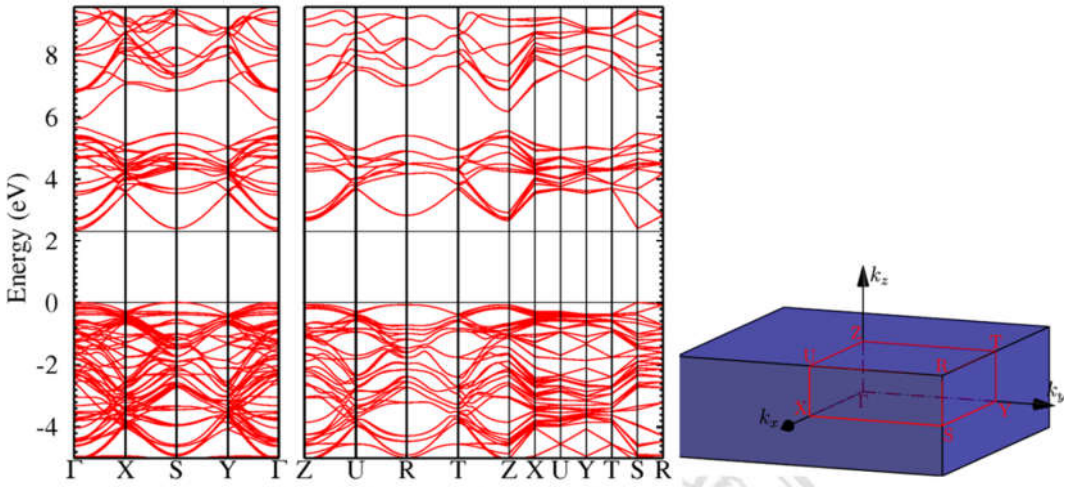

Figure 3.7 (a) The electronic band structure of orthorhombic $NaNbO_3$ along full symmetry path of irreducible Brillouin zone, and (b) irreducible Brillouin zone (bounded by red lines) and the associated high symmetry points (labeled in red) used for band structure calculation. Zero of energy was set as a part of VBM at Γ point.

From Figure 3.7, conduction band minimum (CBM) of $NaNbO_3$ is found to be clearly located at Γ point. For valence band maximum (VBM), the values at either Γ or S could be defined as VBM. Thus, there is no significant difference between the values of indirect and direct band gap in this case. However, our predicted direct band gap of 2.32 eV at Γ point is a little different from previous GGA results of 2.48 eV from Ref. [54]. The discrepancy between the predicted band gap reported in Ref. [54] and from this work probably occurs from the difference in the calculated lattice constants, where their results differ from the experimental data up to 1.6% while our GGA lattice constants match those from experiment within 0.43% discrepancy (the details are presented in Table 4.1). Note that the experimental band gap of orthorhombic $NaNbO_3$ is 3.30 eV [55]. However, our smaller band gap is understandable because ordinary DFT with LDA and GGA implementation has been known to generally underestimate the band gap. To deal with band gap problem, higher level of DFT approach, such as hybrid functional [56] and GW method [57, 58] should be considered. However, this thesis focuses on structural, mechanical, and piezoelectric properties of some perovskites. Their meaningful results can be still figured out using GGA.

Apart from band gap, density of states and projected density of states of $NaNbO_3$ were analyzed as shown in Figure 3.8.

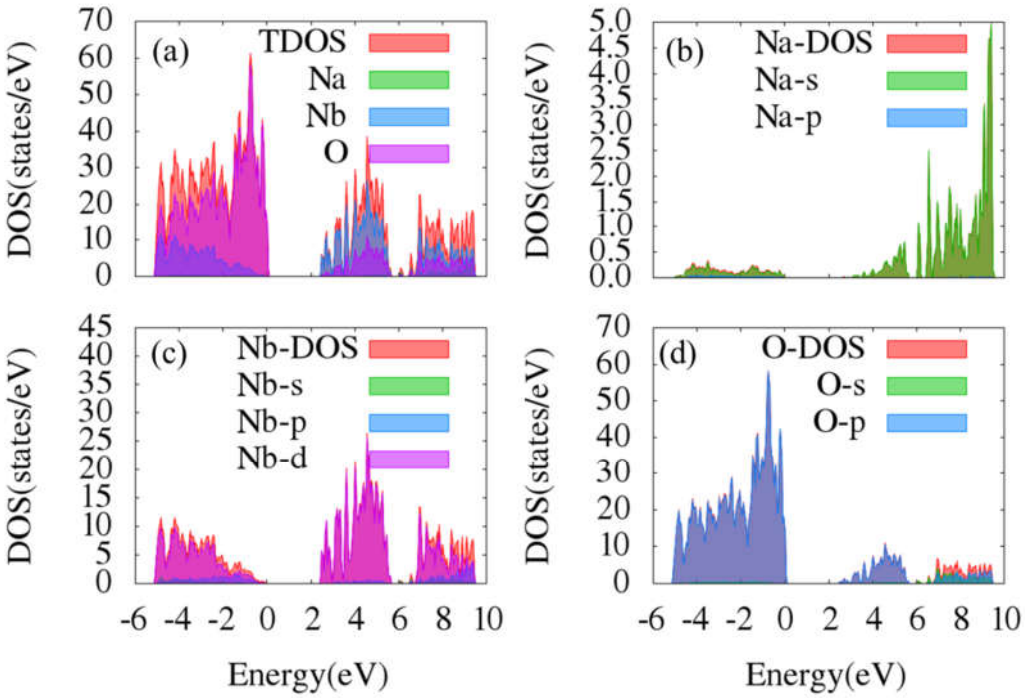

Figure 3.8 Density of states (DOS) of orthorhombic $NaNbO_3$: (a) total DOS and summation of DOS of Na, Nb, and O atoms, (b) DOS of Na atom and its projection onto *s* and *p* orbitals, (c) DOS of Nb atom and its projection onto *s*, *p*, and *d* orbitals, and (d) DOS of O atom and its projection onto *s* and *p* orbitals.

As in the case of $KNbO_3$, alkali metals at A-site of perovskite still provide low contribution to the electronic states near band gap (see Figure 3.8(b)). The main contribution near VBM is from the states of O atoms while Nb atoms provide the main contribution in conduction band region (Figure 3.8 (c-d)). Most of Nb electronic states can be projected onto its 4*d* orbital while 2*p* orbital dominates the electronic states of O near band gap region. Between -6 to -2 eV of energy window, the hybridization (covalence bonding) of Nb 4*d* and O 2*p* can be observed from Figure 3.8. These obtained features of $NaNbO_3$ DOS agree well with the results reported in Ref. [54].

3.3 Electronic structures of $AgNbO_3$

At room temperature, crystal structure of $AgNbO_3$ perovskite is usually found in orthorhombic crystal structure with *Pbcm* space group. It is the same crystal structure as that of $NaNbO_3$. The primitive unit cell of $AgNbO_3$ contains 40 atoms as shown in Figure 3.9.

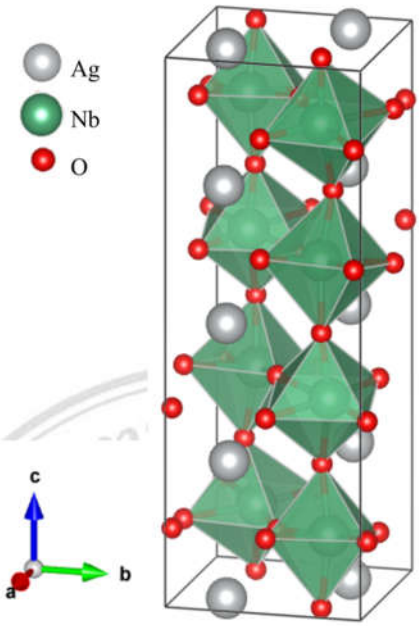

Figure 3.9 Crystal structure of $AgNbO_3$ in *Pbcm* space group. Nb atoms are confined in oxygen octahedral cages, so their displacement can be measured with respect to the surrounding O atoms.

The crystal structure of orthorhombic $AgNbO_3$ shown in Figure 3.9 is obtained from our structural relaxation. The calculation has been performed using the same set of calculation parameters as used in the case of $NaNbO_3$. Namely, the exchange-correlation approximation was treated under the GGA approach. Pseudopotentials from GBRV library were employed. The convergence tests of calculation parameters were also performed as shown in Figure 3.10.

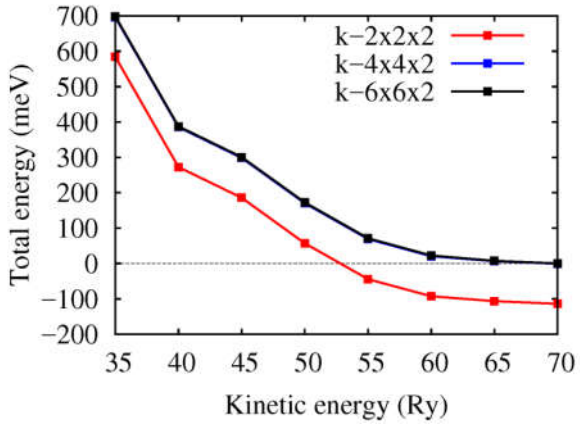

Figure 3.10 The convergence tests of k-point mesh and kinetic energy cutoff with respect to total energy of $AgNbO_3$. The total energy was obtained from the calculation using 6×6×2 k-point mesh and 70 Ry of kinetic energy cutoff was set to zero for conveniences in the comparison.

As seen in Figure 3.10, the variation of total energy with respect to the choice of k-point mesh and kinetic energy cutoff is very similar to the case of $NaNbO_3$. This is because they possess the same crystal structure with *Pbcm* space group. The k-point mesh suitable for $AgNbO_3$ and $NaNbO_3$ crystal structure is then equivalent. There is also no difference of variation in the total energy with respect to kinetic energy cutoff, indicating that the O pseudopotential requires no high energy cutoff for Na or Ag. Hence, the suitable choice of k-point mesh and kinetic energy cutoff for the calculation of this orthorhombic $AgNbO_3$ are 4×4×2 and 60 Ry, respectively.

This convergence set of calculation parameters was then used to calculate electronic band structures of orthorhombic $AgNbO_3$. The obtained results can be represented as shown in Figure 3.11.

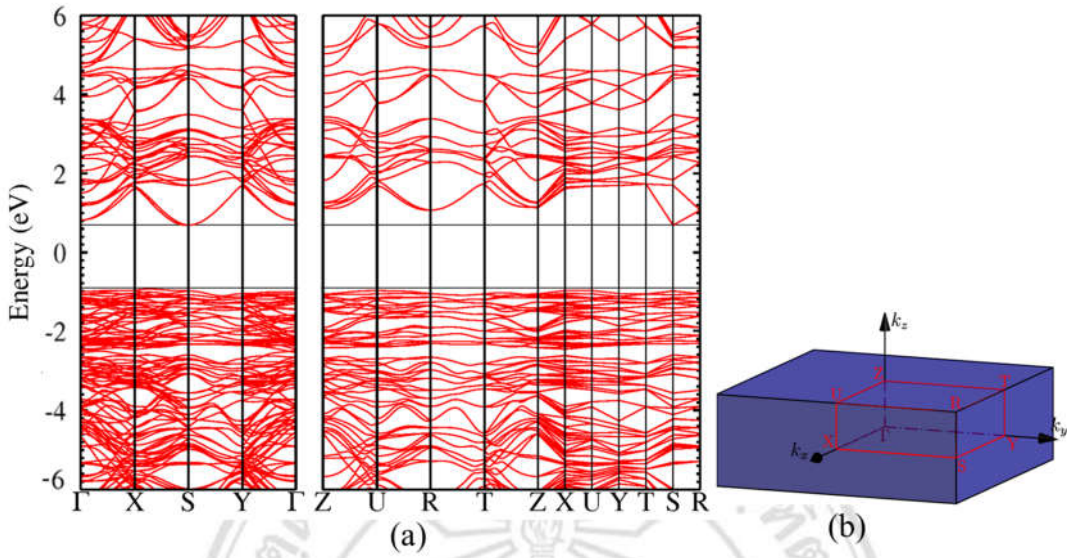

Figure 3.11 (a) The electronic band structure of orthorhombic $AgNbO_3$ along full symmetry path of irreducible Brillouin zone, (b) irreducible Brillouin zone (bounded by red lines) and the associated high symmetry points (labeled in red) used for band structure calculation. Zero of energy was set at the middle of the gap.

From Figure 3.11, band gap of 1.62 eV has been predicted at S point. This value of band gap is smaller than those obtained from $NaNbO_3$ and $KNbO_3$. The CBM obtained at S point is consistent with CBM appearing in band structure of orthorhombic $AgNbO_3$ reported in Ref. [59]. The calculated $AgNbO_3$ band gap of about 3.0 eV reported in Ref. [59] was obtained using hybrid functional. Thus, it cannot be directly compared with our results. Furthermore, several DFT works related to optical properties of $AgNbO_3$ usually emphasizes on the photocatalytic activity [59, 60]. This property requires the accurate calculation of both band gap and band edge [61]. Therefore, hybrid functional in the DFT calculation is often used in the case of $AgNbO_3$. Although Ref. [59] and this work use the different exchange interaction, other features of band structure, such as the strong dispersion of CBM on X-S-Y plane, are still consistent.

To further investigate the electronic contribution to the states near band gap, density of states and projected density of states of $AgNbO_3$ were analyzed as shown in Figure 3.12.

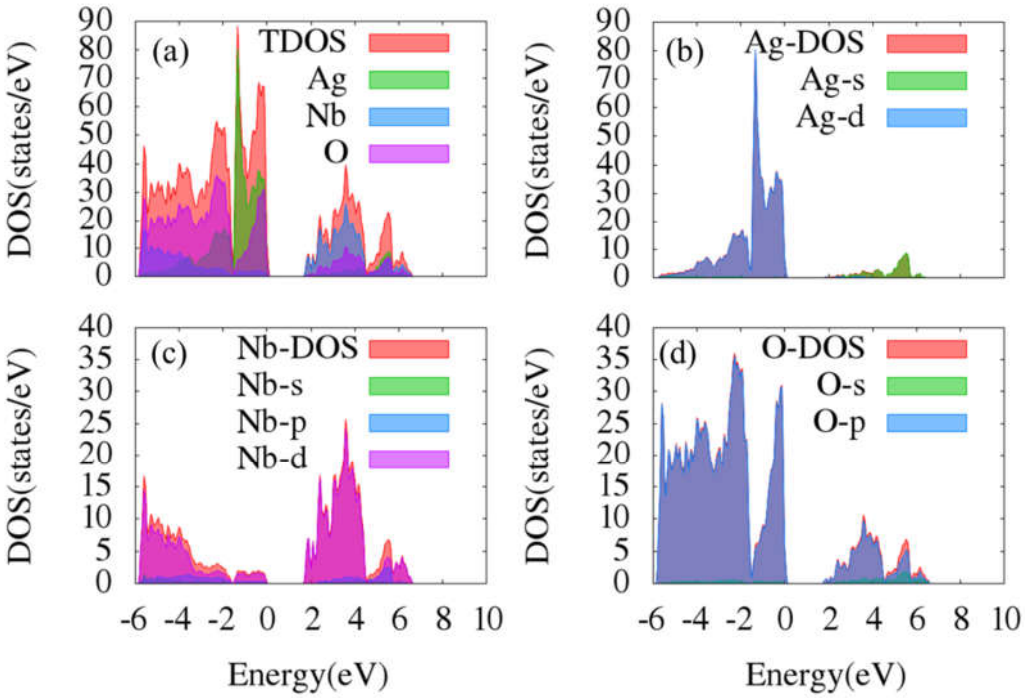

Figure 3.12 Density of states (DOS) of $AgNbO_3$ in *Pbcm* phase : (a) total DOS and summation of DOS of Ag, Nb, and O atoms, (b) DOS of Ag atom and its projection onto *s* and *d* orbitals, (c) DOS of Nb atom and its projection onto *s*, *p*, and *d* orbitals, and (d) DOS of O atom and its projection onto *s* and *p* orbitals.

From DOS analysis of $AgNbO_3$, A-site cation (Ag atom) also provides the contribution to the states near VBM, which cannot be observed in the case of $KNbO_3$ and $NaNbO_3$. Therefore, valence band of $AgNbO_3$ is formed mainly by the presence of the Nb 4*d*, Ag 4*d* and O 2*p* states. It is also found that both Ag 4*d* and O 2*p* have peaks near VMB region, indicating the strong hybridization between Ag 4*d* and O 2*p*. Chemical and physical properties of $AgNbO_3$ are then not governed by only the hybridization between Nb 4*d* and O 2*p* states but also Ag 4*d*. Because this difference in electronic structure of $AgNbO_3$ compared with both $KNbO_3$ and $NaNbO_3$, $AgNbO_3$ probably exhibit novel and attractive properties.

3.4 Electronic structures of $BiGaO_3$

$BiGaO_3$ perovskite has been predicted to be stable in tetragonal phase with *P4mm* symmetry [22]. Its primitive unit cell contains 5 atoms as shown in Figure 3.13.

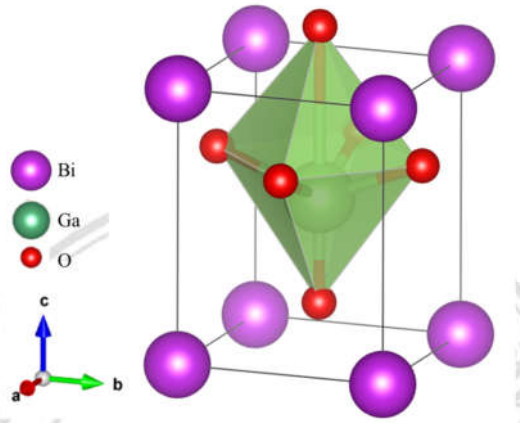

Figure 3.13 Crystal structure of $BiGaO_3$ in *P4mm* space group. Ga atom is confined in oxygen octahedral cages, so their displacement can be measured with respect to the surrounding O atoms.

The crystal structure of $BiGaO_3$ shown in Figure 3.13 has been relaxed to its equilibrium structure, where the net force applied to each atom is zero. The structural relaxation of tetragonal $BiGaO_3$ was performed within the converged calculation parameters. To acquire the converged calculation parameters, it should be noted that the small supercell (5 atoms) requires high density of k-point. The kinetic energy cutoff for both Bi and Ga atoms was also carefully tested, where the results can be shown in Figure 3.14. In the figure, the converged values of k-point mesh and kinetic energy cutoff with respect to total energy of this tetragonal $BiGaO_3$ is 4×4×4 and 60 Ry, respectively. This convergence set was then used to calculate electronic band structures of tetragonal $BiGaO_3$. The obtained results can be presented as shown in Figure 3.15.

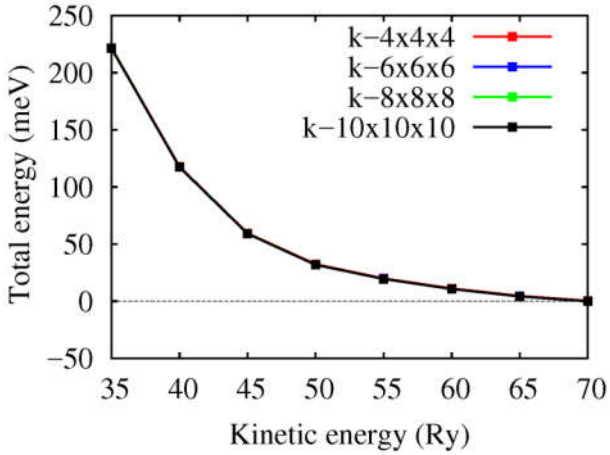

Figure 3.14 The convergence tests of k-point mesh and kinetic energy cutoff with respect to total energy of $BiGaO_3$. The total energy was obtained from the calculation using 10×10×10 k-point mesh and 70 Ry of kinetic energy cutoff was set to zero for conveniences in the comparison.

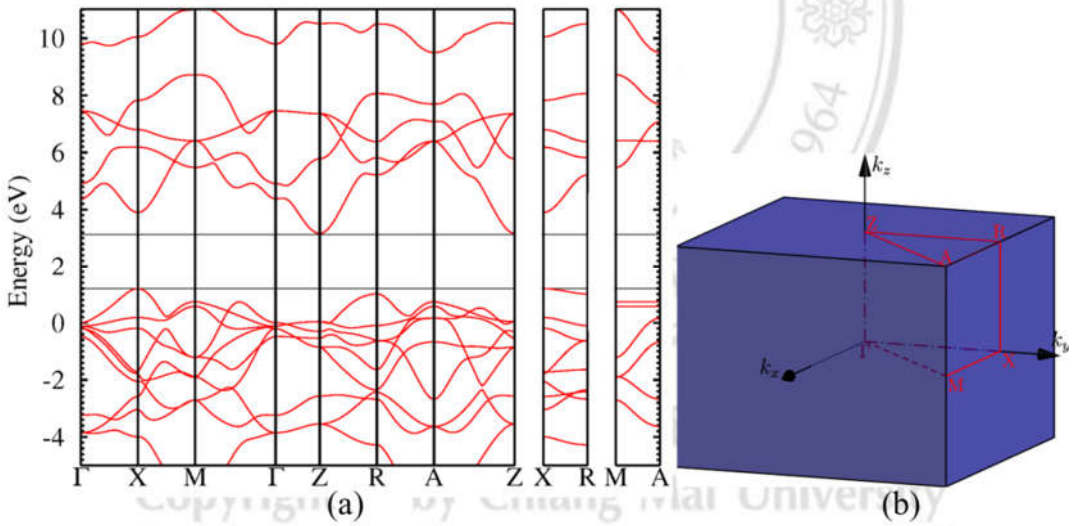

Figure 3.15 (a) The electronic band structure of tetragonal $BiGaO_3$ along full symmetry path of irreducible Brillouin zone, (b) irreducible Brillouin zone (bounded by red lines) and the associated high symmetry points (labeled by red) used for band structure calculation. Zero of energy was set as a part of VBM at Γ point.

Electronic band structures of tetragonal $BiGaO_3$ reveals that the acquired VBM and CBM are located at X and Z point, respectively. Thus, band gap of $BiGaO_3$ in *P4mm* phase is indirect. Surprisingly, although tetragonal $BiGaO_3$ exhibits very high

spontaneous polarization, the report about electronic band structures of this phase is rare. The available data of band gap based on GGA calculations are for cubic and orthorhombic phases which the values are 1.91 eV [62] and 1.88 eV [63], respectively. For tetragonal phase studied in this work, the value of 1.93 eV is found. Interestingly, the values of band gap of $BiGaO_3$ in different phases predicted by GGA are comparable.

Apart from band gap calculation, the contribution of electronic states near band gap of tetragonal $BiGaO_3$ was also investigated via density of states and projected density of states analysis as shown in Figure 3.16.

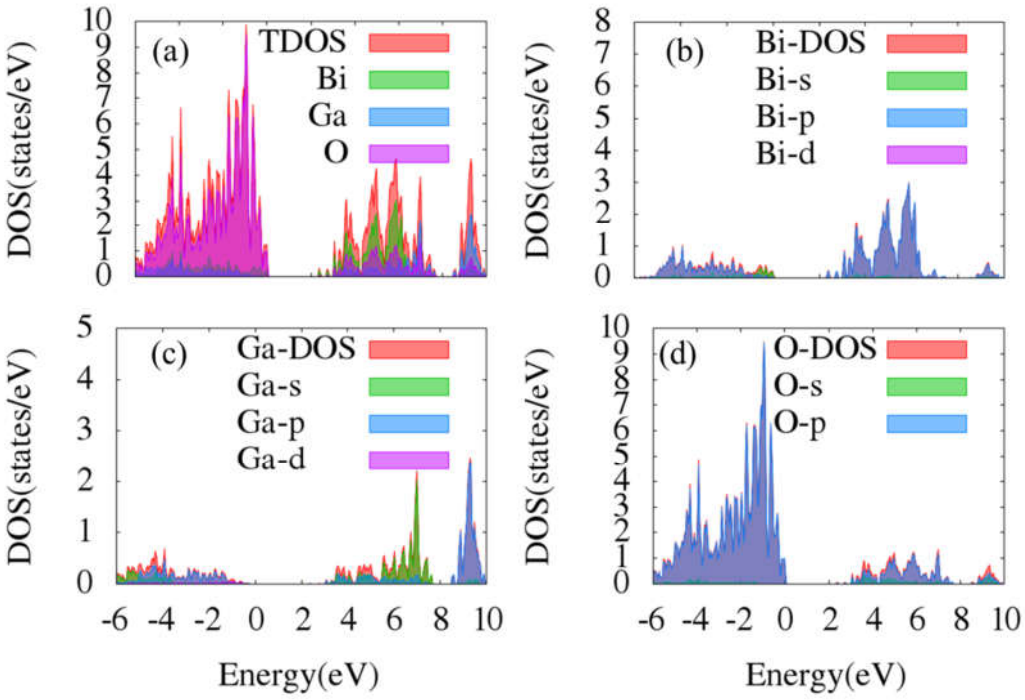

Figure 3.16 Density of states (DOS) of tetragonal $BiGaO_3$: (a) total DOS and summation of DOS of Bi, Ga, and O atoms, (b) DOS of Bi atom and its projection onto *s*, *p*, and *d* orbitals, (c) DOS of Ga atom and its projection onto *s*, *p*, and *d* orbitals, and (d) DOS of O atom and its projection onto *s* and *p* orbitals.

In contrast to the cases of $KNbO_3$, $NaNbO_3$, and $AgNbO_3$, cation at B-site, i.e. Ga, has less contribution to the states around band gap compared with that of Nb cation in former cases. Most of electronic states of Bi can be projected onto its 6*p* orbital. However, it has been known that electrons in 6*s* orbital of Bi are lone pair and responsible for the large displacement of B-site cation (see Figure 3.13), resulting in the

large polarization. Therefore, in Bi-based perovskite, the main mechanism that allows superior ferroelectricity is not from hybridization (or covalent bonding) between B-site cation and the O anion, but from the stereochemically active 6*s* lone pair electrons of Bi ion. The presence of 6*s* states can be observed at VBM as shown in Figure 3.16(b).

3.5 Electronic structures of $BiAlO_3$

At room temperature $BiAlO_3$ adopts rhombohedral crystal structure with *R3c* space group. Its primitive unit cell contains 10 atoms (two formulas) as shown in Figure 3.17.

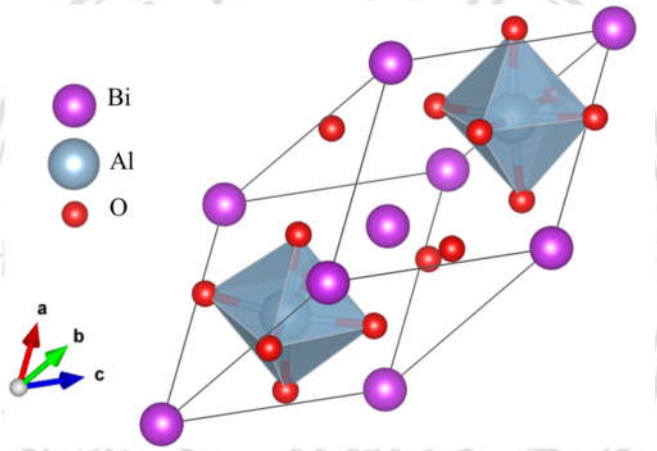

Figure 3.17 Crystal structure of $BiAlO_3$ in *R3c* space group. Al atom is confined in oxygen octahedral cages, so their displacement can be measured with respect to the surrounding O atoms.

$BiAlO_3$ perovskite in *R3c* space group is the only one crystal structure studied in this research that possesses non-orthogonal lattice vector (see Figure 3.17). The convergence tests of k-point mesh and kinetic energy cutoff with respect to total energy can be presented in Figure 3.18. From the figure, using 4×4×4 k-point mesh and 60 Ry of kinetic energy cutoff for the calculation of rhombohedral $BiAlO_3$ provide the converged results. With these calculation parameters, electronic structure calculation of rhombohedral $BiAlO_3$ was then performed. The results of band structure calculation can be found in Figure 3.19.

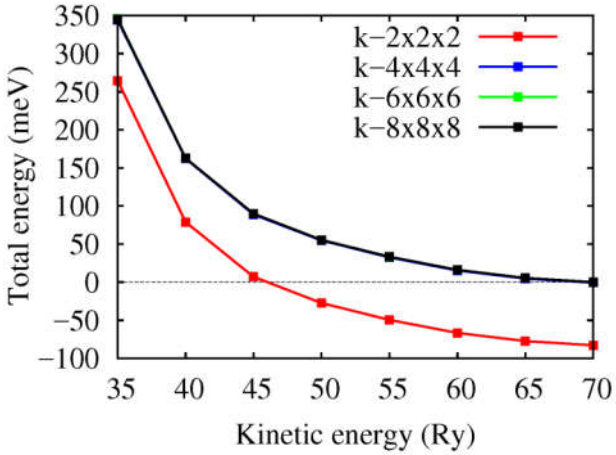

Figure 3.18 The convergence tests of k-point mesh and kinetic energy cutoff with respect to total energy of $BiAlO_3$. The total energy was obtained from the calculation using 8×8×8 k-point mesh and 70 Ry of kinetic energy cutoff was set to zero for convenience in the comparison.

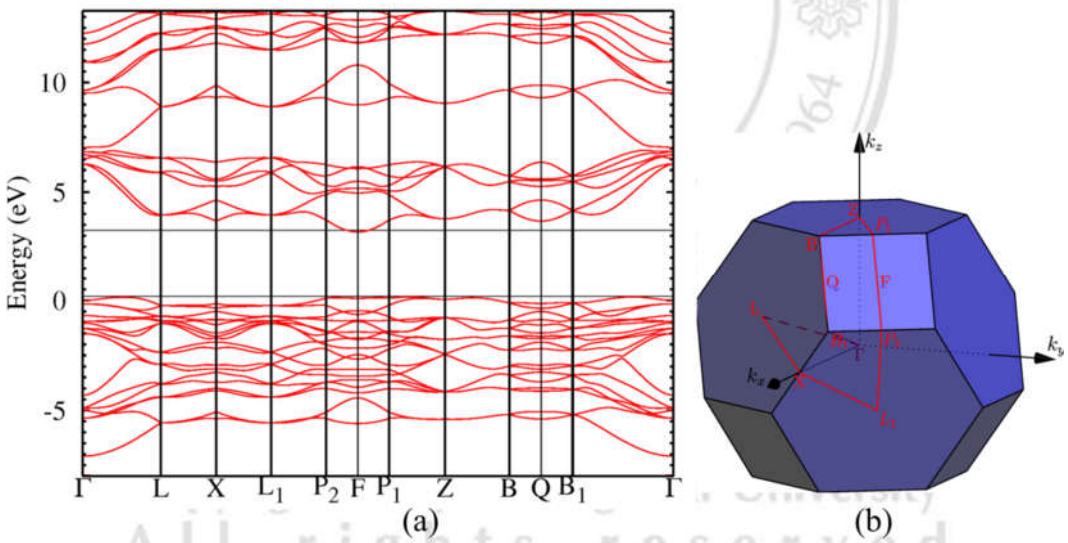

Figure 3.19 (a) The electronic band structure of $BiAlO_3$ in *R3c* phase along full symmetry path of irreducible Brillouin zone, and (b) the irreducible Brillouin zone (bounded by red lines) and the associated high symmetry points (labeled by red) used for band structure calculation. Zero of energy was set as a part of VBM at Γ point.

As is seen, the predicted band gap of 3.05 eV in this case is the largest value compared with those from $KNbO_3$, $NaNbO_3$, $AgNbO_3$, and $BiGaO_3$. This results exhibit a good agreement with the band gap of 3.00 eV and 2.90 eV reported in Ref. [64] and

Ref. [65], respectively. Band structure along high symmetry path between Γ and L points, represented in Fig. 2 of Ref. [64] can be directly compared with our results, suggesting the consistency.

To further investigate the electronic contribution to the states near band gap, density of states and projected density of states of $BiAlO_3$ were analyzed as shown in Figure 3.20.

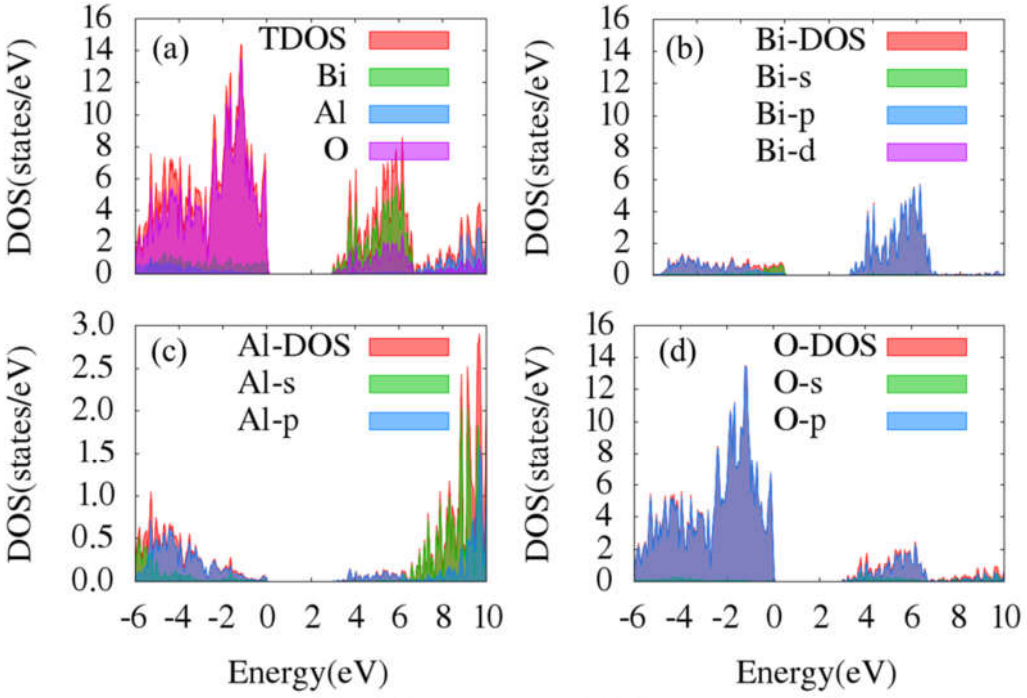

Figure 3.20 Density of states (DOS) of $BiAlO_3$ in *R3c* phase : (a) total DOS and summation of DOS of Bi, Al, and O atoms, (b) DOS of Bi atom and its projection onto *s*, *p*, and *d* orbitals, (c) DOS of Al atom and its projection onto *s* and *p* orbitals, and (d) DOS of O atom and its projection onto *s* and *p* orbitals.

As found in the case of $BiGaO_3$, B-site cation provide low contribution to the electronic state near band gap. The peaks of Al-DOS in both valence band and conduction band are low compared with total DOS (TDOS). The occurrence of 6*s* lone pair on Bi atom near VBM is also observed in this case. The similarity between DOS of $BiGaO_3$ and $BiAlO_3$ indicates the significant role of 6*s* lone pair found in Bi-based perovskites.